High Density Operation in Pulsator

Pulsator Group[+)]

presented by O. Klüber

IPP III/21 März 1976

MAX-PLANCK-INSTITUT FÜR PLASMAPHYSIK

8046 GARCHING BEI MÜNCHEN

MAX-PLANCK-INSTITUT FÜR PLASMAPHYSIK

GARCHING BEI MÜNCHEN

High Density Operation in Pulsator

Pulsator Group[+)]

presented by O. Klüber

IPP III/21 März 1976

[+)] B. Cannici, W. Engelhardt, J. Gernhardt, E. Glock, F. Karger, O. Klüber, G. Lisitano, H.M. Mayer, D. Meisel, P. Morandi, S. Sesnic, F. Wagner.

Die nachstehende Arbeit wurde im Rahmen des Vertrages zwischen dem Max-Planck-Institut für Plasmaphysik und der Europäischen Atomgemeinschaft über die Zusammenarbeit auf dem Gebiete der Plasmaphysik durchgeführt.

IPP III/21

High Density Operation in Pulsator

Pulsator Group

Presented by O. Klüber

März 1976

Abstract

This report summarizes the results of experiments at high electron densities ($> 10^{14} cm^{-3}$) which have been achieved by pulsed gas inflow during the discharge. At these densities a regime is established which is characterized by $\beta_p > 1$, $n_i \sim n_e$, $T_i \sim T_e$ and $\tau_E \propto n_e$. Thus the toroidal magnetic field contributes considerably to the plasma confinement and the ions constitute almost half of the plasma pressure. Furthermore, the confinement is appreciably improved and the plasma becomes impermeable to hot neutrals.

1.) Introduction

Most Tokamak discharges last longer than the particle confinement time which means that, in the absence of other sources, lost particles must be recycled from the wall. Assuming a recycling coefficient of 1, the density is expected to be proportional to the filling pressure. Experiments on Pulsator show, however, that only the density reached in the first 0.5 ms follows this expectation. Generally after 20 ms a steady-state value is reached which can be higher or lower than the filling density, depending on the discharge current and on the vacuum conditions. Frequent opening of the torus, for example, may lead to a plateau density which is more than five times the filling density. On the other hand, during a series of 2000 shots where no opening took place, the plateau density decreased continuously, so that the value $1.5 \times 10^{13} cm^{-3}$ has not been exceeded regardless of the filling pressure. These observations led us to the conclusion that the recycling coefficient of hydrogen is less than 1. In order to control the density in an independent way and moreover to lower the relative impurity content, experiments have been started to replace lost hydrogen by pulsed gas inflow.

The experimental setup is shown in Fig. 1. Access to the torus is provided by four ducts which are connected to the vacuum pumps via large conduits. In the steady-state filling mode hydrogen is slowly pumped through the torus. Pulsed gas inflow is provided by a volume of $\sim 50\ cm^3$ filled with hydrogen in the torr range which is expanded by a fast acting valve into one of the conduits from where the gas enters the torus. Thus, the particle flux is given by

$$\Phi = \Phi_o \left(e^{-\frac{t}{\tau_1}} - e^{-\frac{t}{\tau_2}} \right)$$

where $\tau_1 \sim 50$ ms, $\tau_2 \sim 5$ ms.

The first results presented at the Lausanne Conference /1/ revealed some very promising features, especially a decrease of Z_{eff} and an increase in β_p and in the energy replacement time τ_E. Since then the performance has been appreciably improved: As reported at the St. Petersburg APS meeting and published in Nuclear Fusion /2/ the following data have been attained: $n_e(o) = 1.7 \ 10^{14} cm^{-3}$. $\beta_p = 1.5$, $Z_{eff} = 1.9$, $\tau_E = 10$ ms (with a plasma radius of 11 cm). It is most remarkable that these data were achieved at the rather small q value of 3.5.

In the following the properties of these plasmas are described in some more detail, especially the temporal evolution of the T_e and n_e profiles and the stability behaviour . Futhermore, some experiments with different parameters are discussed and the results are compared with numerical simulations using the Düchs code.

2.) Temporal evolution of the plasma parameters

The time dependence of the plasma current, loop voltage, electron line density, peak electron temperature and ion temperature is shown in Fig. 2. The toroidal magnetic field is 27 kG giving a minimum q(a) of 3.3 at the maximum current of 66 kA. The gas inflow starts at t = 40 ms. Some ms later a hump in the loop voltage appears with a maximum at t = 51 ms. This time agrees well with the time when the neutral flux attains its maximum. The amplitude of the voltage hump increases with increasing initial slope of the density trace which in this case is $3 \cdot 10^{12} cm^{-3} (ms)^{-1}$. The hump becomes undetectable if the density rise is more than a factor of 2 slower. This voltage hump is due to a shrinking and expansion of the current channel. This is seen by comparing the T_e profiles shown in Figs. 3, 4 and 5. It is clearly seen that between t = 44 ms and t = 51 ms the outer regions of the plasma column are appreciably cooled whereas the central region retains its tem-

perature. It should be stated that the authors do not claim that the T_e profile at t = 51 ms has really a minimum at the centre. The time at which the voltage maximum appears has some jitter. Though it is small this will obviously have a strong influence on the T_e profile at a fixed time near the maximum of the loop voltage. Furthermore, the saw-tooth-like modulation of the electron temperature in the central region deteriorates the reproducibility. Between t = 51 ms and t = 60 ms the outer regions are only slightly cooled but the central temperature decreases strongly. For the sake of comparison, the T_e profiles at t = 44, 51 and 60 ms are plotted again in Fig. 7. It is seen from this figure that the electron temperature drop between t = 51 ms and t = 60 ms occurs at r < 3 cm. The skin time constant $\tau = \mu_o \delta r_o^2/2$ amounts τ = 7 ms with r_o = 3 cm and the δ value corresponding to kT_e = = 1 keV and Z_{eff} = 4.

The same τ value is obtained with r_o = 6 cm and kT_e = 400 eV, these data being representative for the outer regions where the temperature decrease occurs between t = 44 ms and t = 51 ms. It is possible, therefore, that the variation of the T_e profiles leads to an according variation of the current density distribution. At the same time when the hump appears, the plasma current decreases slightly. Thus the loop voltage

$$u = u_\Omega + \frac{d}{dt}(\mathcal{L}\mathcal{I})$$

with

$$\mathcal{L} = \mu_o R \left(\ln \frac{\hat{r}_o}{a} + \frac{\ell_i}{2} \right)$$

(U_Ω being the ohmic voltage, $\hat{r}_o$ the radius of magnetic surface at which U is measured) is given by

$$u = u_\Omega + \mathcal{L} \frac{d\mathcal{I}}{dt} + \mu_o R \mathcal{I} \frac{d}{dt} \frac{\ell_i}{2}$$

The peak value of LdI/dt is -0.3 V. If $dl_i/2\,dt$ is replaced by $\Delta l_i/2\Delta t = 0.1/7$ ms the last term amounts 0.8 V giving 0.5 V

for the resulting amplitude of the voltage hump. This agrees well with the measured hump amplitude of 0.4 V.

The decrease in the electron temperature is accompanied by a sharp rise of the ion temperature as can be seen from Fig.2 and more distinctly from Fig. 8 where the same curve is plotted in a more extended scale. T_i increases from 190 eV at 50 ms to 280 eV at 60 ms. The reason for this sharp jump is obviously the enhanced energy transfer from the electrons to the ions on account of the increasing electron density and the decreasing electron temperature. Beyond $t = 60$ ms the measured ion temperature increases only slightly. This may be partially due to the fact that with rising electron density the contribution from the plasma centre to the observed neutral flux decreases. As already stated in Ref. /2/, the actual peak ion temperature may be larger than the value deduced by the neutral flux.

The process of peaking and flattening of the T_e profile exhibits some resemblance to the phenomenon known as "internal disruption"; it is indeed easily detectable by the surface-barrier X-ray diodes as is shown in Fig. 9. It extends, however, over a much larger fraction of the plasma cross section and occurs - correspondingly - on a much larger time scale. Obviously, the basic process is quite a different one, namely the cooling of the plasma column due to the penetration of neutrals into the plasma core. At least in a transient phase the source term for ionization is more or less peaked somewhere between the edge and the centre which manifests itself in the off-centre maxima of the n_e profiles (c.f.Figs. 4 and 6).

From the T_e profiles the q profiles have been calculated using the usual assumption that Z_{eff} is constant over the plasma radius. These calculations give a central value of $q(0) < 1$ only for 45 ms $< t <$ 75 ms. This result remains still valid if the effect of trapped electrons is taken into account.

(These calculations have been performed by P. Smeulders.) In contrast to these findings, however, the m = 1, n = 1 oscilations and the sawtooth-like m = 0, n = 0 internal disruptions are observed during the whole discharge. To solve this contradiction, it must be assumed that the current density profile is more peaked than that calculated under the assumption that Z_{eff} is constant over the plasma radius.

This view is reinforced by the radial profiles of the X-ray spectra. These results and a detailed analysis of the diode measurements are dealt with in Ref. /3/.

3.) Disruptive end of the discharge

The increase of β_p due to the pulsed gas inflow leads to outward displacement of the plasma column and hence to the onset of disruption if the vertical magnetic field is not adjusted properly. In some cases the discharges described in Figs. 2 to 9 could be kept stable. More frequently, however, the current terminates due to a disruptive instability at t > 100 ms which at this time could not be avoided by adjusting the vertical field. It was already stated in Ref. /2/ that in this case there is a close connection between the time when the disruption occurs and the impurity content in the discharge. This is again shown in Fig. 10 where the emission of the O VI line λ = 1032 Å is plotted as a function of time for four subsequent shots. For comparison the emission of H_α at the location of the gas inflow is also plotted. From shot to shot the initial peak increases which indicates that each discharge leaves the wall in a progressively different state with respect to the release of oxygen. Furthermore, after starting the gas inflow the increase of the O VI signal becomes steeper from shot to shot. It has been observed that, apparently as a result, the disruption

occurs earlier from shot to shot. The enhanced emission of the O VI line during the density rise is at least only partially due to an enhanced inflow of oxygen which could be caused by enhanced plasma-wall interaction due to the increasing density. This is clearly demonstrated by the time behaviour of oxygen lines arising from lower states of ionization, as can be seen from Fig. 11 where the intensities of these oxygen lines are plotted. The intensities of all lines are normalized to the value they attain at $t = 40$ ms, i.e. the time when the gas inflow starts. If one assumes that enhanced inflow of oxygen is the only reason for the increasing line emission all line traces should have had the same slope. From this and from the observation that the increase in the line emission occurs first in O VI we conclude that recombination is at least partially if not totally responsible for the enhanced line emission. Since the oxygen contamination increases from shot to shot as it is indicated by the increase of the initial peak, the radiative cooling increases also. This may lead to a progessively faster shrínkage of the current channel and hence to the observed deterioration of the stability.

The onset of disruptions can be postponed by a small number of pulse cleaning shots which lead to a reduction of the oxygen content. This reduction manifests itself in a reduction of the initial peak and of the slope in the O VI emission curve. The onset is also postponed by a small reduction of the hydrogen influx in which case of course the cooling is also slightly reduced.

There is, however, a quite different possible explanation based on theoretical considerations by H. Wobig /4/. It is shown there that azimuthally localized particle sources - as they are established by the pulsed gas inflow - may lead to convective cells if at least two ion species are present in the plasma. Such cells are expected to be en-

hanced by magnetic islands originating at resonant magnetic surfaces and may be regarded to be the initial mechanism for the onset of the disruptive instability. So far the theory is not fully developed but its basic features fit quite well to the observed phenomena. The decisive role of magnetic islands for the onset of the disruptive instability has been clearly demonstrated by earlier experiments on Pulsator /5, 6/.

It should be pointed out that the disruptive instabilities at high density exhibit all the phenomena which are well known from low density Tokamak discharges, in particular the increase of the MHD modes (preferrably of the type $m = 2$, $n = 1$), some ms before disruption, the negative voltage spike, and the sudden inward displacement of the plasma column.

During the stable period between the start of the gas inflow and the disruptive termination, the Mirnov probe signals are appreciably reduced, typically by a factor 3 as compared to the level before the density rise. Nevertheless, stable operation at q values lower than 3.5 could not be achieved at densities above $10^{14}\,cm^{-3}$ peak value, whereas at smaller densities q values down to 2.2 have been attained.

4.) Variation of parameters

The power supply allows a maximum toroidal magnetic field of only 27 kG if a flat-top time of more than 100 ms is desired. Thus, the influence of an increase in q(a) can only be studied by reducing the plasma current. At $I = 40$ kA which corresponds to $q(a) = 5.5$ a β_p value of 1.5 could not be exceeded for two flow rates different by a factor of two. On the other hand, $\beta_p = 1.5$ could also be attained at $I = 40$ kA, $B = 17$ kG which again gives $q(a) = 3.5$.

In all discharges described above the plasma current was kept approximately constant in time. (cf.Fig.2). In a further experiment a decrease of the plasma current from 66 kA to 40 kA was artificially induced by opening a circuit parallel to the primary winding. In this case a β_p value of 2 was reached. The temporal evolution of the plasma current and of β_p are shown in Fig. 12. For $t > 40$ ms four β_p curves are plotted: the contribution β_{pe} of the electrons as calculated from the T_e and n_e profiles, the value $2\,\beta_{pe}$ giving an upper limit, the value $\beta_p(1 + \frac{T_i}{T_e})$, where T_i is the measured ion temperature and $\beta_{p\Delta}$. $\beta_{p,\Delta}$ was obtained from the signals of the magnetic position probes which allow for the determination of $\beta_p + \ell_i/2$. The normalized inductance ℓ_i was calculated assuming a current density profile proportional to $T_e^{3/2}(r)$. The absolute error in $\ell_i/2$ which may be caused by this assumption is less than 0.1. Thus it can be stated that at $t = 90$ ms a β_p value of 2 has been attained. It is quite surprising that the peak electron temperature and the T_e profile differ only slightly from that in the case of constant current which is shown in Fig. 6.

From all these data it must be inferred that there is no simple relationship between the maximum attainable β_p value and q(a). It must be stated that the plasma radius in all cases is defined by $a = a_L - /\Delta /$ where $a_L = 11$ cm is the limiter radius and Δ the displacement of the plasma column. Δ is deduced from the readings of the magnetic probes and amounts typically 0.5 cm or less. The effective plasma radius, however, may be markedly smaller than this value, depending on the heating and the cooling of the outer regions which obviously varies with the flow rate. Thus a possible existing dependence may be masked.

In all discharges investigated so far, the ratio of the ion temperature as it was deduced from the charge-exchange neutral spectra to the peak electron temperature was typically

0.6. The actual peak ion temperature may still be closer to $T_e(0)$, because in all cases the central electron density was above $10^{14}\,cm^{-3}$. Furthermore, Z_{eff} ranges between 1.75 and 2.25 for all discharges. This means that n_i/n_e is almost 1 even if oxygen is assumed to be the only present impurity. From these data it follows that $p_i > 0.6\ p_e$.

5.) Comparison with the Düchs code

The Pulsator discharge described in section 3 has been simulated by the six-regime Tokamak transport code developed by D.F. Düchs et al. /7/. This code allows for several generations of charge-exchange neutrals and for the presence of one impurity species; in this case oxygen was chosen. The criteria deciding on the transport coefficients are those used for the simulation of the usual Tokamaks plasmas at lower densities. The calculated data fit the measured ones surprising well, even in such details like the occurrence of the hump in the loop voltage and the sharp increase of the ion temperature. This can be seen from Fig. 13 where the measured U and T_i curves are the same as in Figs. 2 and 8, respectively. Fig. 14 shows the temporal evolution of the electron line density (cf.Fig.2) and of β_p, Figs. 15 and 16 shows the T_e and n_e profiles at $t = 60$ ms and $t = 90$ ms. (cf. Fig.6).

The agreement between the measured and the calculated curves lends confidence that this code contains important parts of the relevant physics. In particular, it is noteworthy, that up to peak electron densities of almost $2 \cdot 10^{14}\,cm^{-3}$ the density increase can be explained by penetration of the neutrals due to classical processes. A more detailed analysis of the data will be given in a subsequent paper /8/.

Acknowledgement

The authors are greatly indebted to Dr. D.F. Düchs for continuous cooperation and many helpful discussions.

References:

/1/ W. Engelhardt et al., Proc. 7th European Conference on Controlled Fusion and Plasma Physics, Lausanne 1975, Vol. 1, 136.

/2/ O. Klüber et al., Nucl. Fusion 15, 1194, (1975).

/3/ S. Sesnic, IPP III/22

/4/ H. Wobig, Verhandlungen der Deutschen Physikalischen Gesellschaft, 2, paper P24, 203, (1976).

/5/ F. Karger et al., Proc. 5th Conference on Plasma Physics and Controlled Nuclear Fusion Research, Tokyo 1974, Vol. I, 207.

/6/ O. Klüber, Proc. 7th European Conference on Controlled Fusion and Plasma Physics, Lausanne 1975, Vol. 2, 50.

/7/ D. F. Düchs, H. Furth, P. Rutherford, Proc. 6th Conference on Controlled Fusion and Plasma Physics, Moscow 1973, Vol. 2, 326.

/8/ D. F. Düchs, IPP report.

Figure Captions

Fig. 1: Schematic view of the vacuum setup.

Fig. 2: Plasma current, loop voltage, electron line density, electron and ion temperature as function of time.

Fig. 3: Electron temperature and density profile at t = 44 ms.

Fig. 4: Electron temperature and density profile at t = 51 ms.

Fig. 5: Electron temperature profiles at t = 30, 60 and 90 ms.

Fig. 6: Electron density profiles at t = 30, 60 and 90 ms.

Fig. 7: Electron temperature profiles at t = 44, 51 60 ms.

Fig. 8: Ion temperature measured via neutral spectra as function of time.

Fig. 9: Signals from the surface-barrier X-ray diodes.

Fig.10: O VI line emission for four successive shots. The emission at the beginning and at the end of the discharge increases from shot to shot. The emission of H_α is proportional to the flow rate of the neutral gas.

Fig.11: Emission of O III, O IV, O V and O VI lines as function of time. All intensities are normalized to the value at t = 40 ms when the gas inflow starts.

Fig.12: Plasma current and β_p as function of time for artificially induced current decrease.

Fig.13: Loop voltage and ion temperature as function of time.———— measured, ... calculated.

Fig.14: Electron line density and β_p as function of time.———— measured, ... calculated.

Fig.15: Electron temperature profiles at t = 60 ms and t = 90 ms.———— measured, ... calculated.

Fig.16: Electron density profiles at t = 60 ms and t = 90 ms.———— measured,.... calculated .

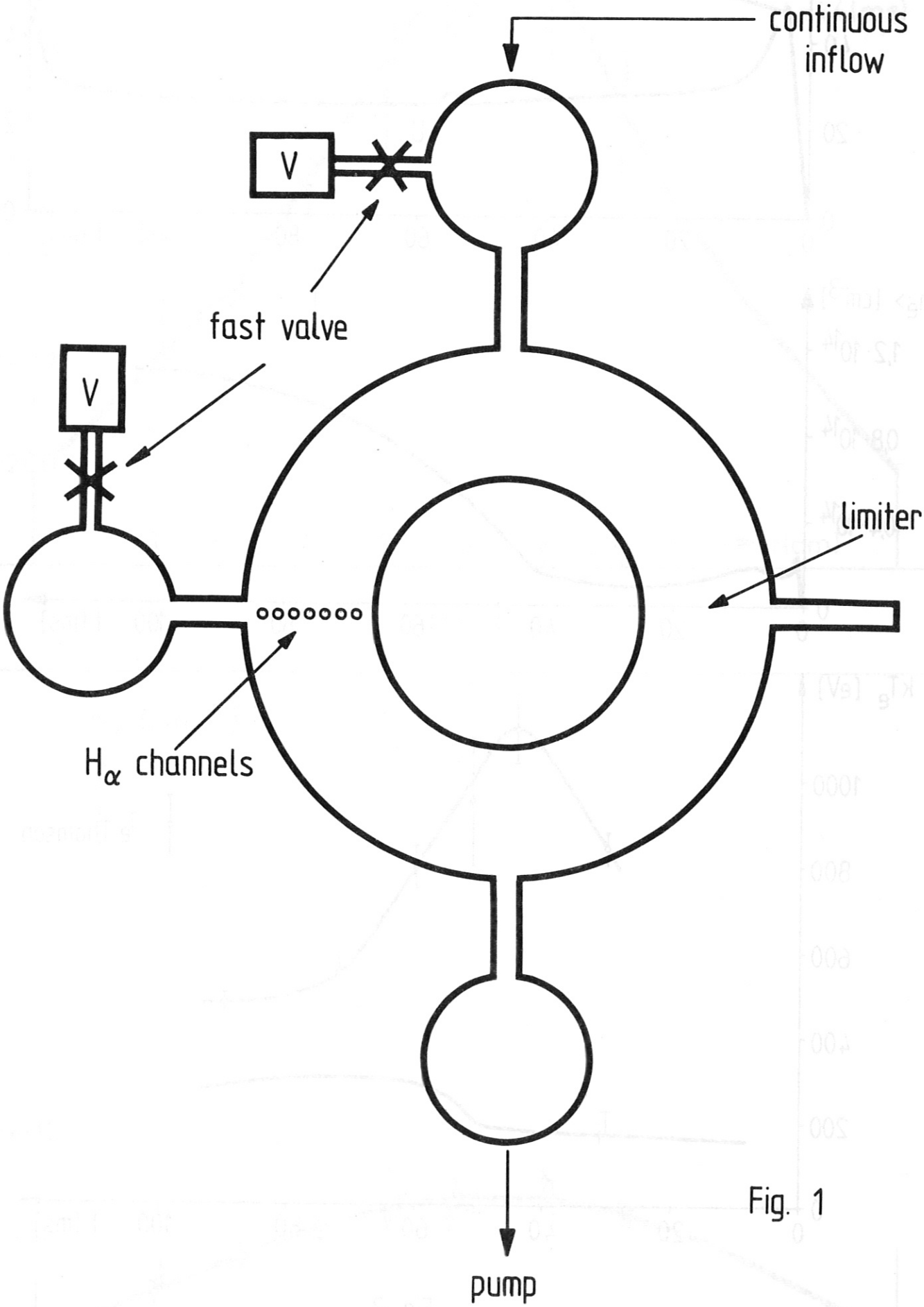
continuous
inflow
V
fast valve
V
limiter
H_α channels
pump

Fig. 1

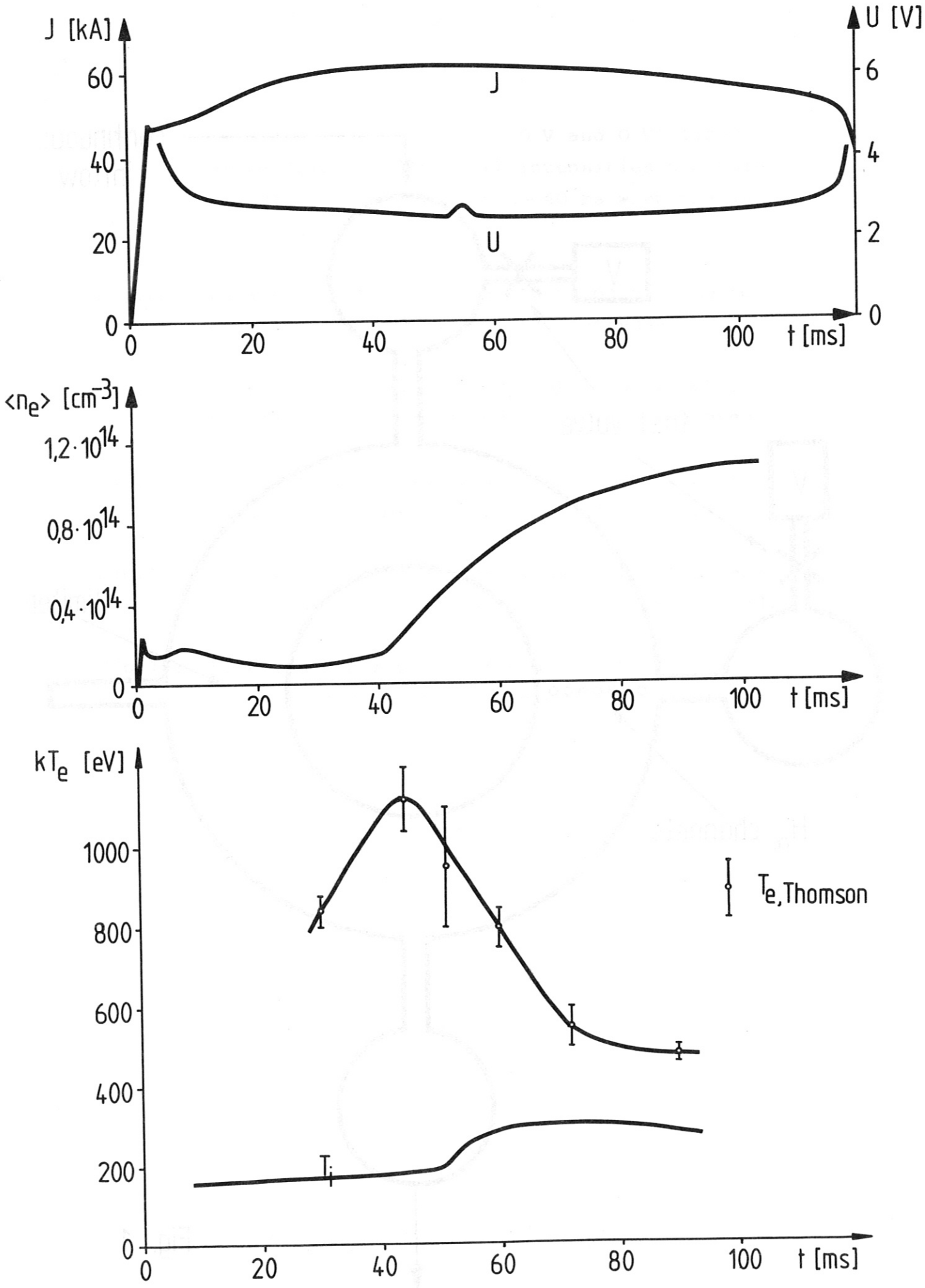
J [kA]
U [V]
60
40
20
0
6
4
2
0
J
U
0
20
40
60
80
100
t [ms]
<ne> [cm⁻³]
1,2·10¹⁴
0,8·10¹⁴
0,4·10¹⁴
0
kTe [eV]
1000
800
600
400
200
Te, Thomson
Ti

Fig. 2

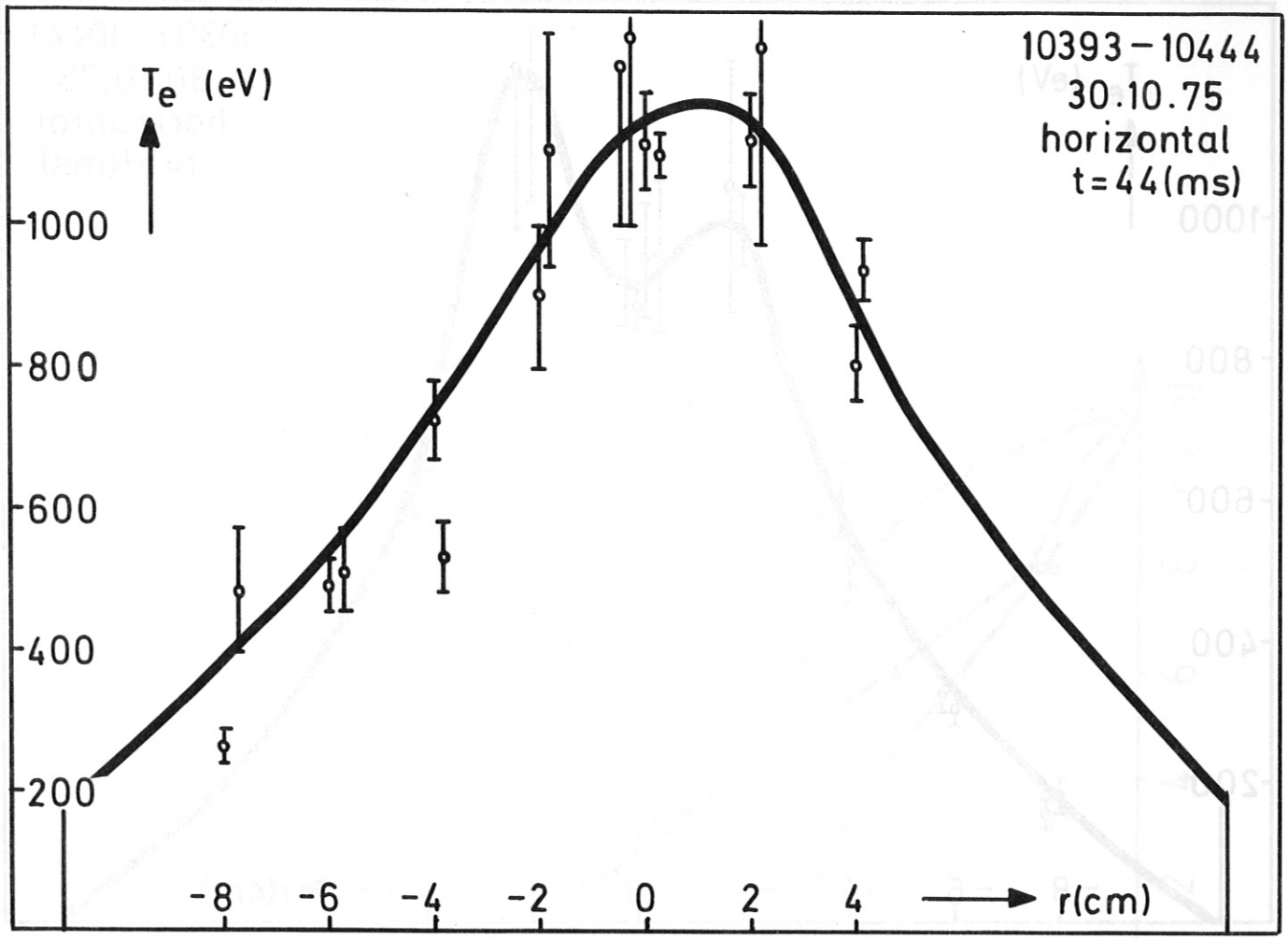
10393 – 10444
30.10.75
horizontal
t = 44 (ms)
T_e (eV)
1000
800
600
400
200
-8
-6
-4
-2
0
2
4
r(cm)

Fig. 3

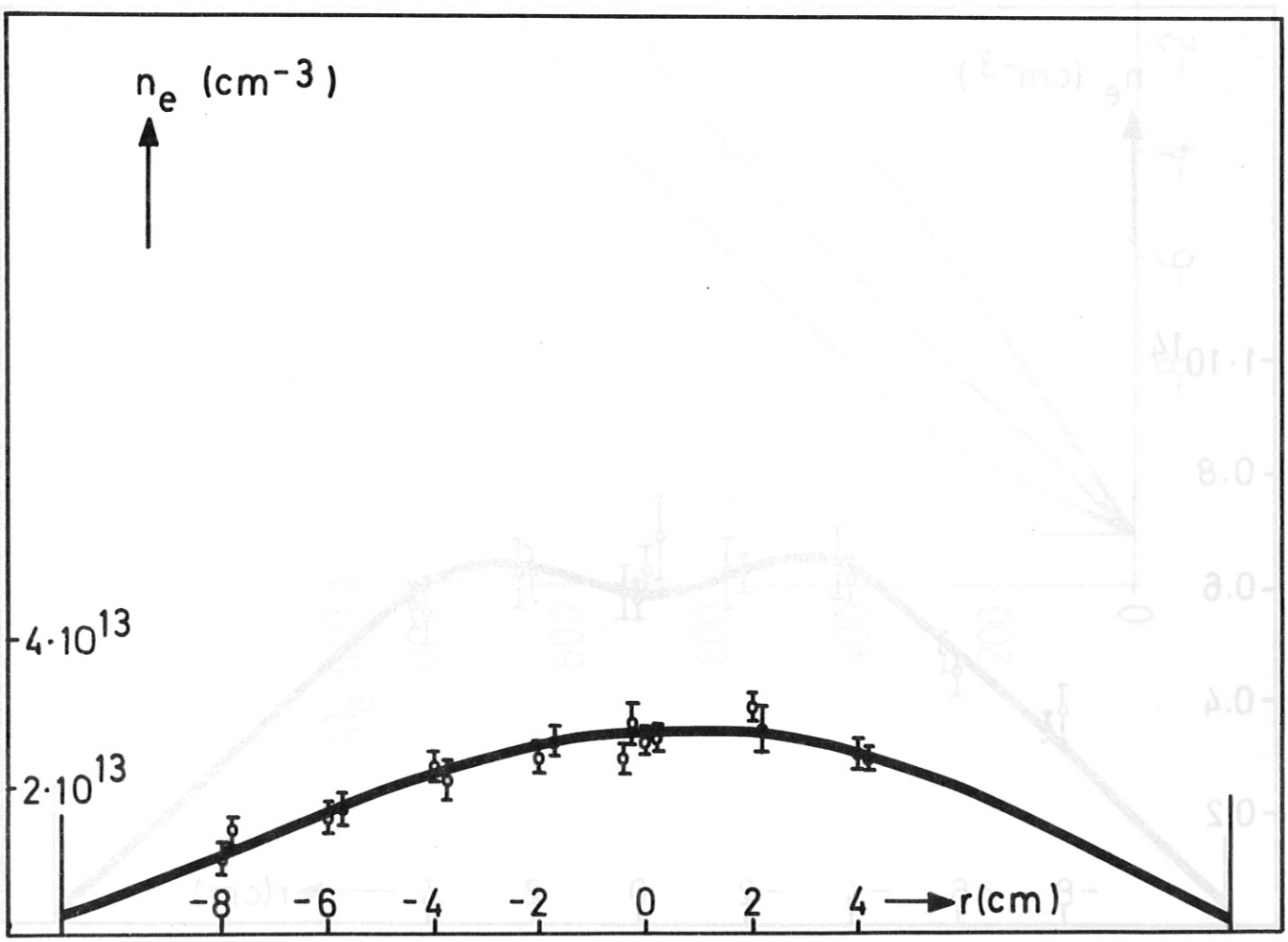
n_e (cm^{-3})
$4 \cdot 10^{13}$
$2 \cdot 10^{13}$
-8
-6
-4
-2
0
2
4
r(cm)

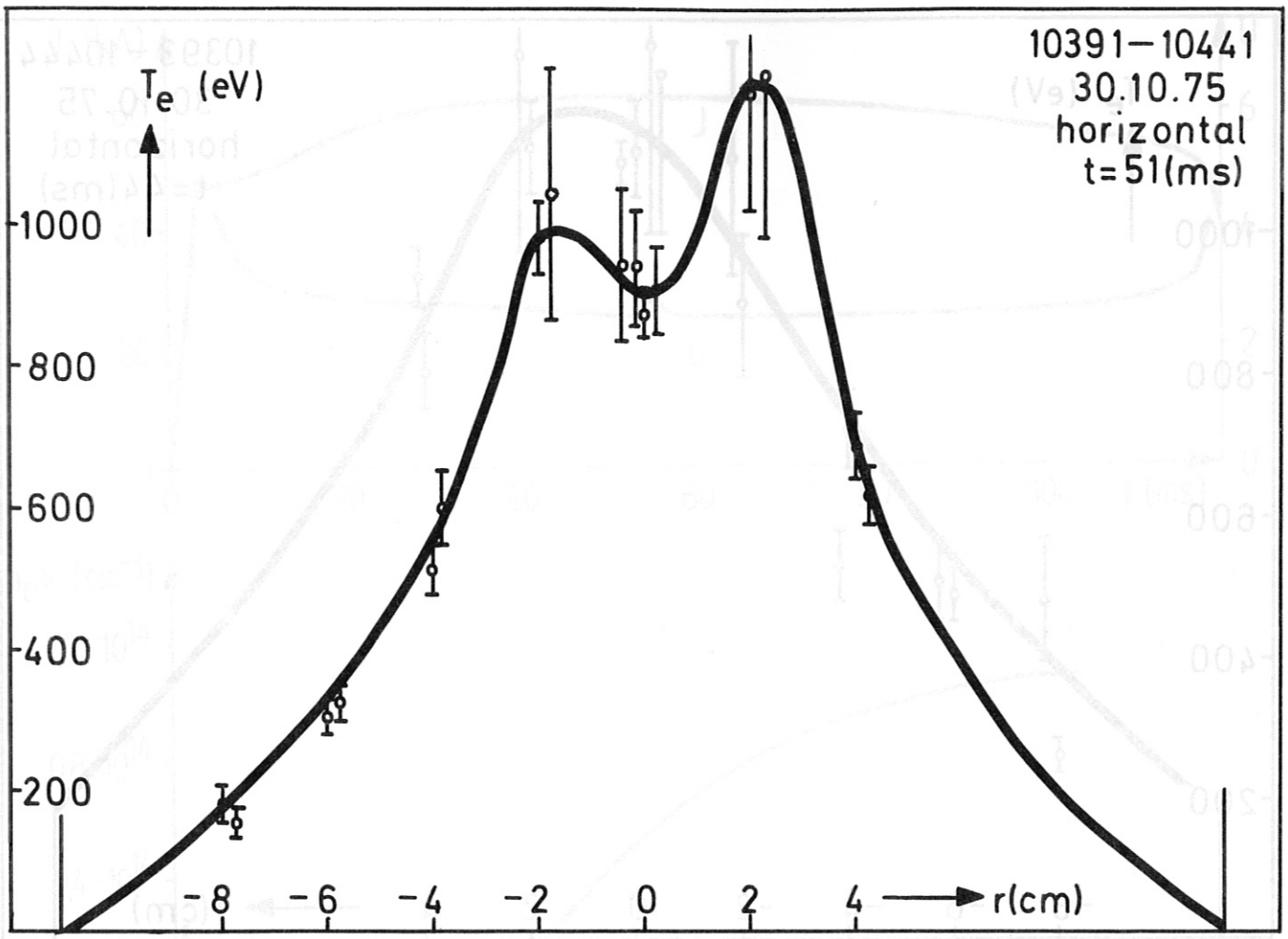
10391–10441
30.10.75
horizontal
t=51(ms)
T_e (eV)
1000
800
600
400
200
-8
-6
-4
-2
0
2
4
r(cm)

Fig. 4

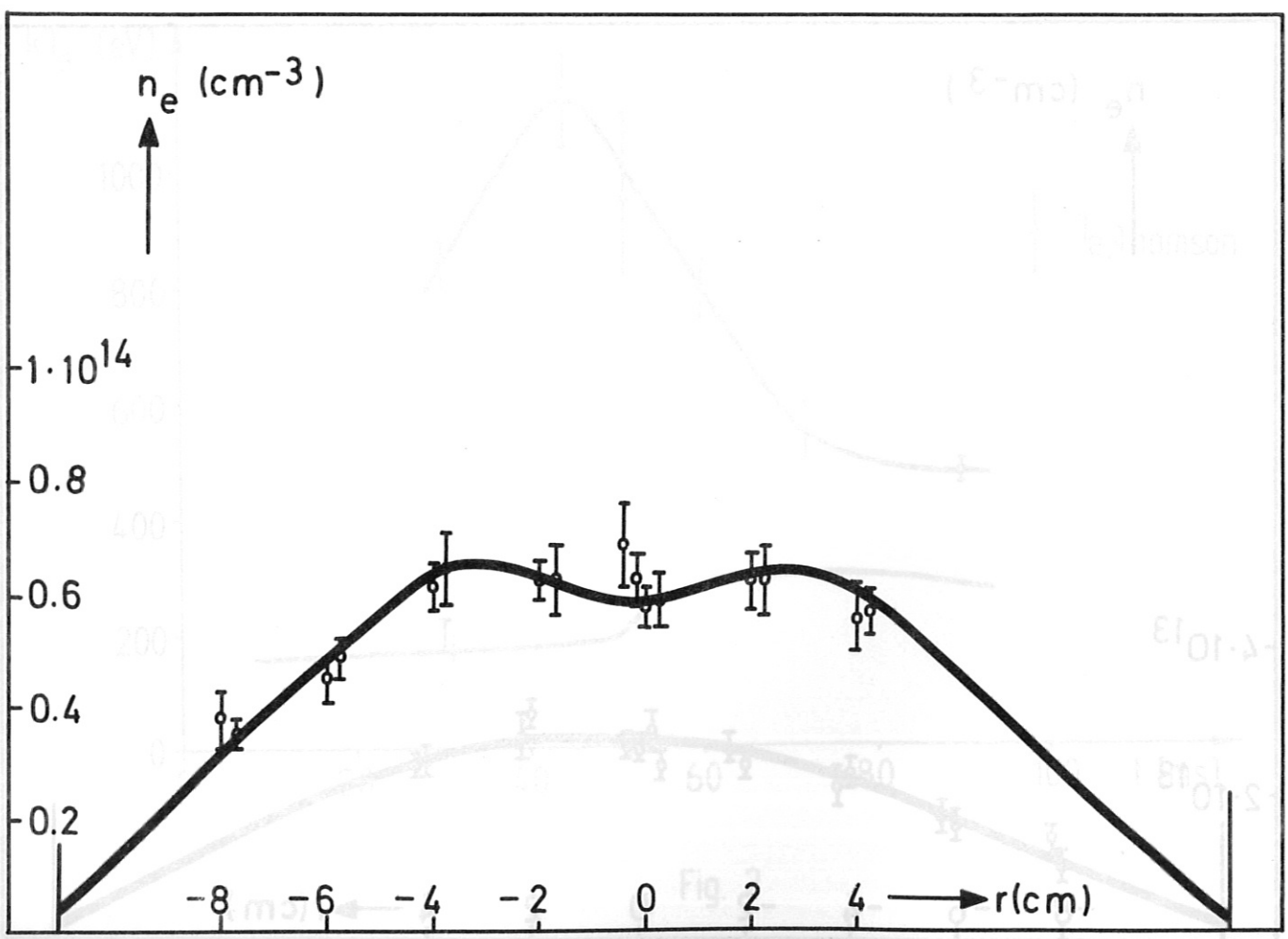
n_e (cm^{-3})
$1 \cdot 10^{14}$
0.8
0.6
0.4
0.2
-8
-6
-4
-2
0
2
4
r(cm)

Fig. 5

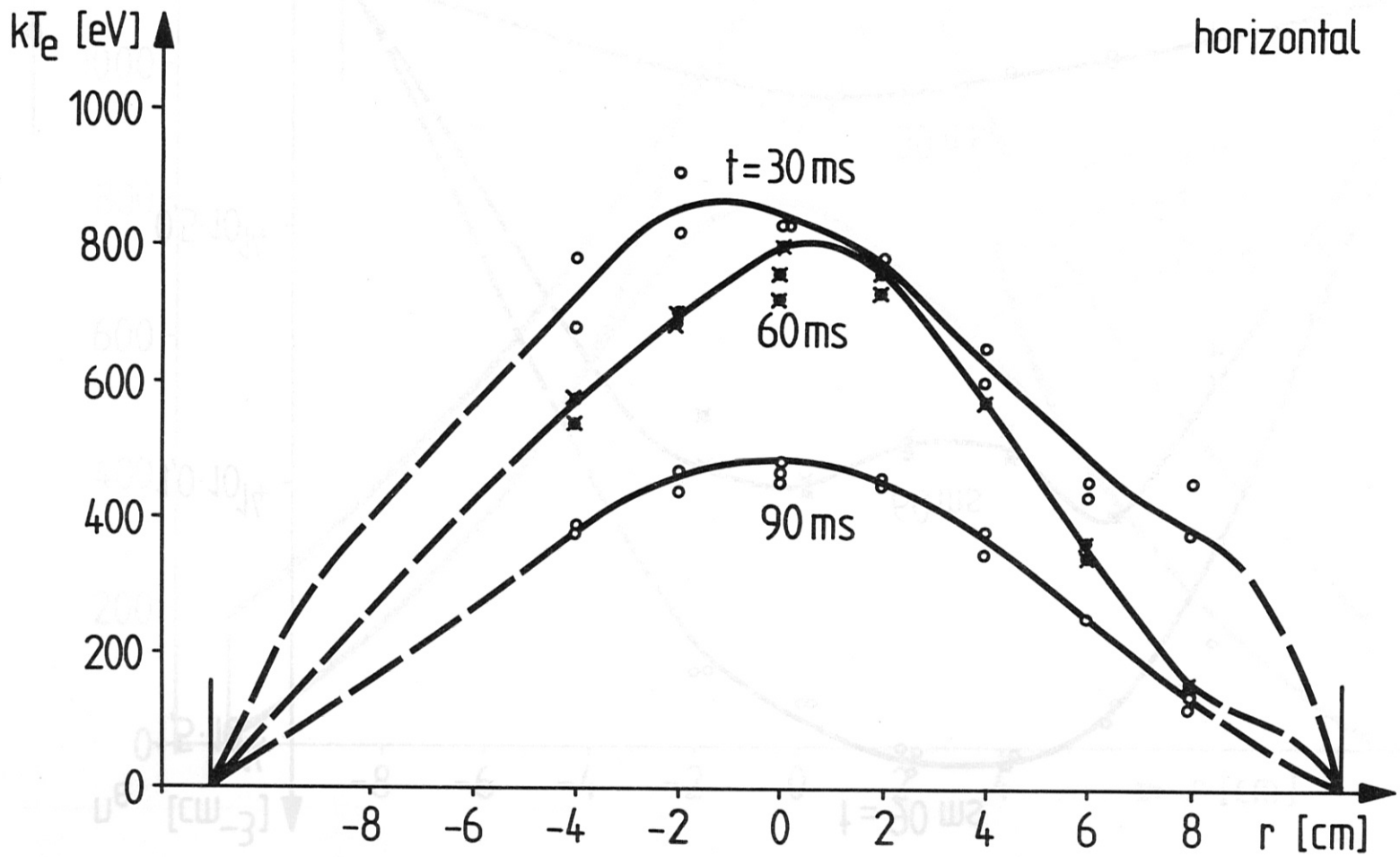
kTe [eV]
horizontal
1000
800
600
400
200
0
t=30ms
60ms
90ms
-8
-6
-4
-2
0
2
4
6
8
r [cm]

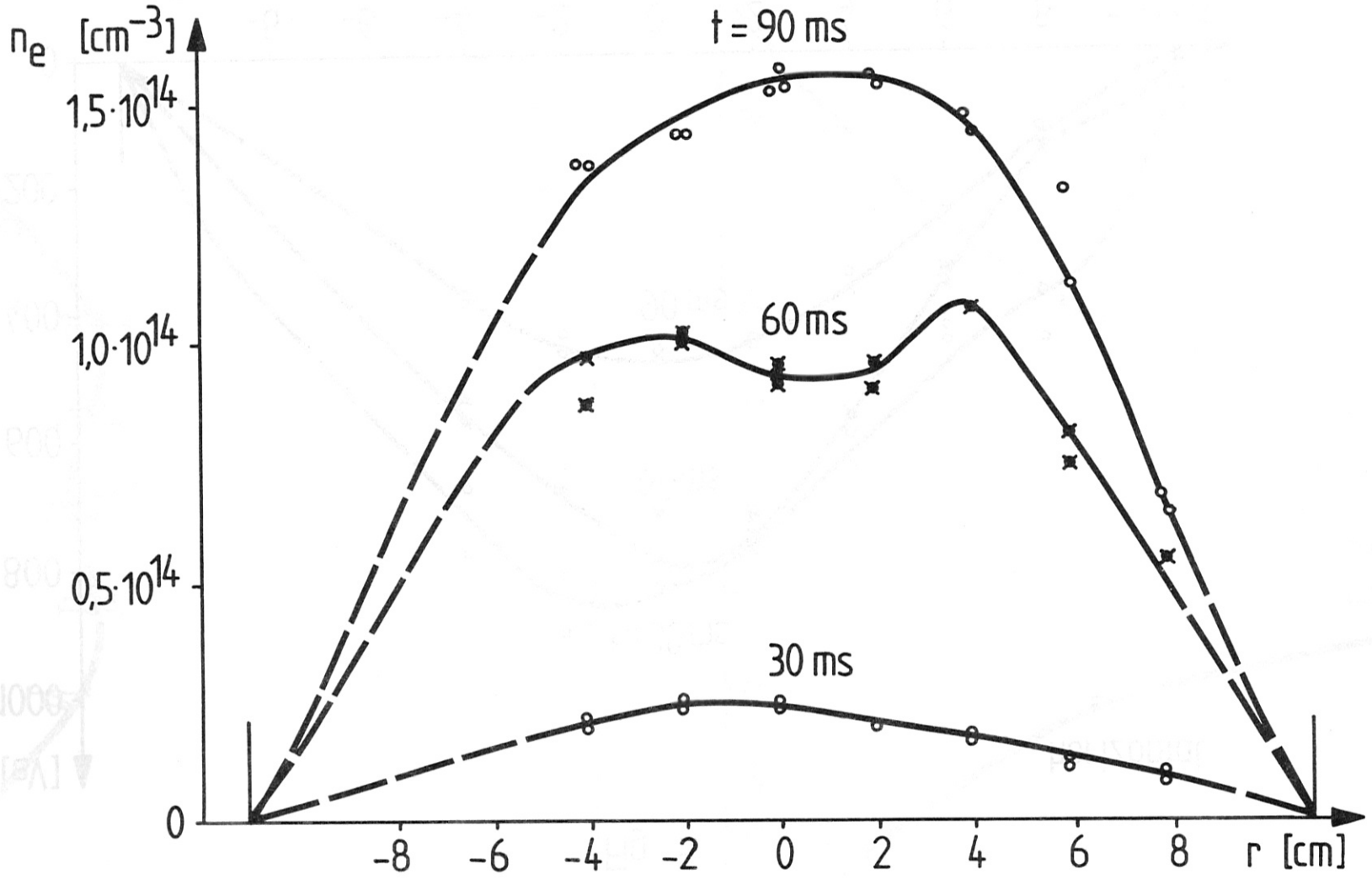
n_e [cm^{-3}]
$1{,}5 \cdot 10^{14}$
$1{,}0 \cdot 10^{14}$
$0{,}5 \cdot 10^{14}$
0
t = 90 ms
60 ms
30 ms
-8
-6
-4
-2
0
2
4
6
8
r [cm]

Fig. 6

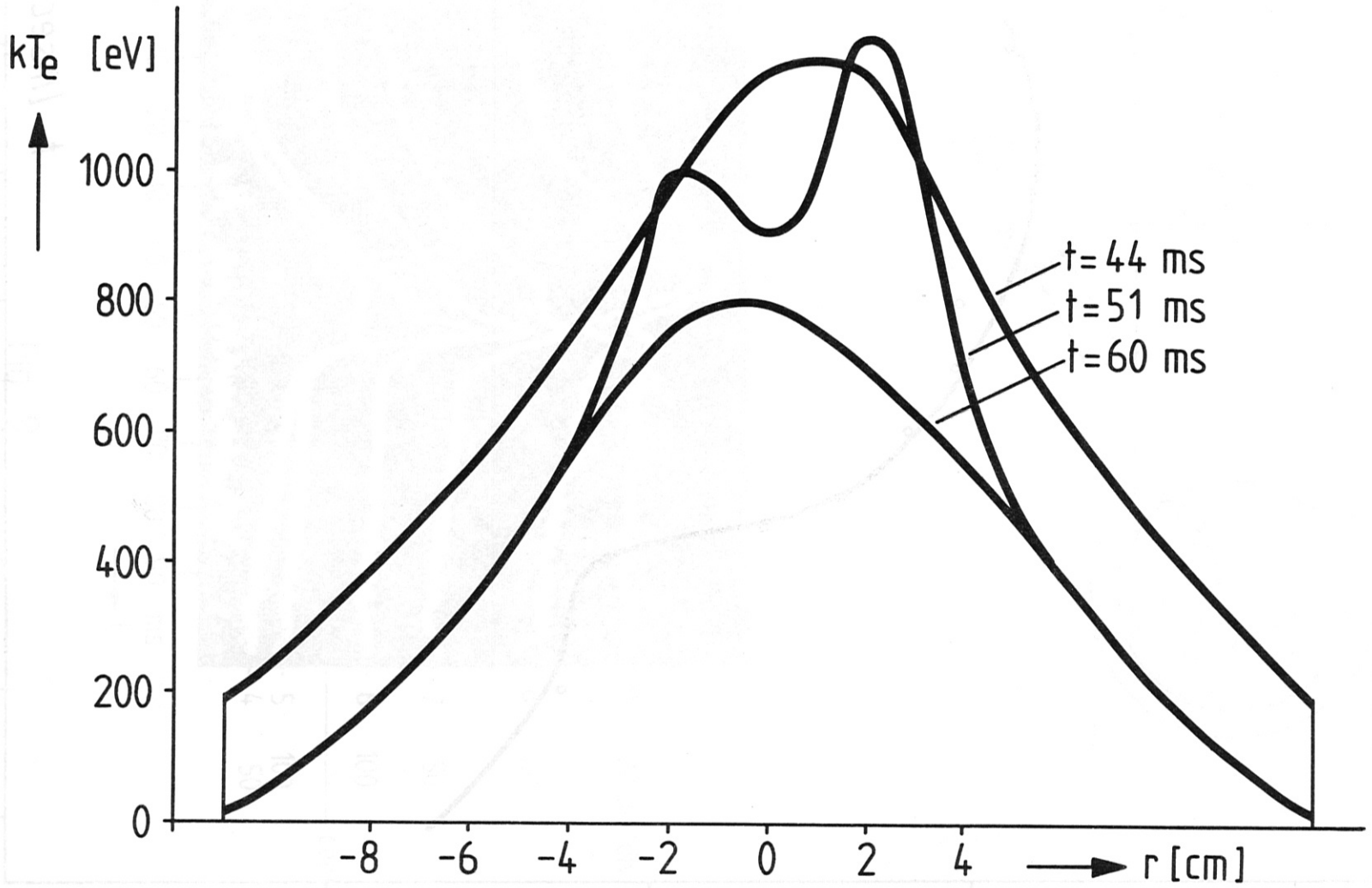

Fig. 7

Fig. 8

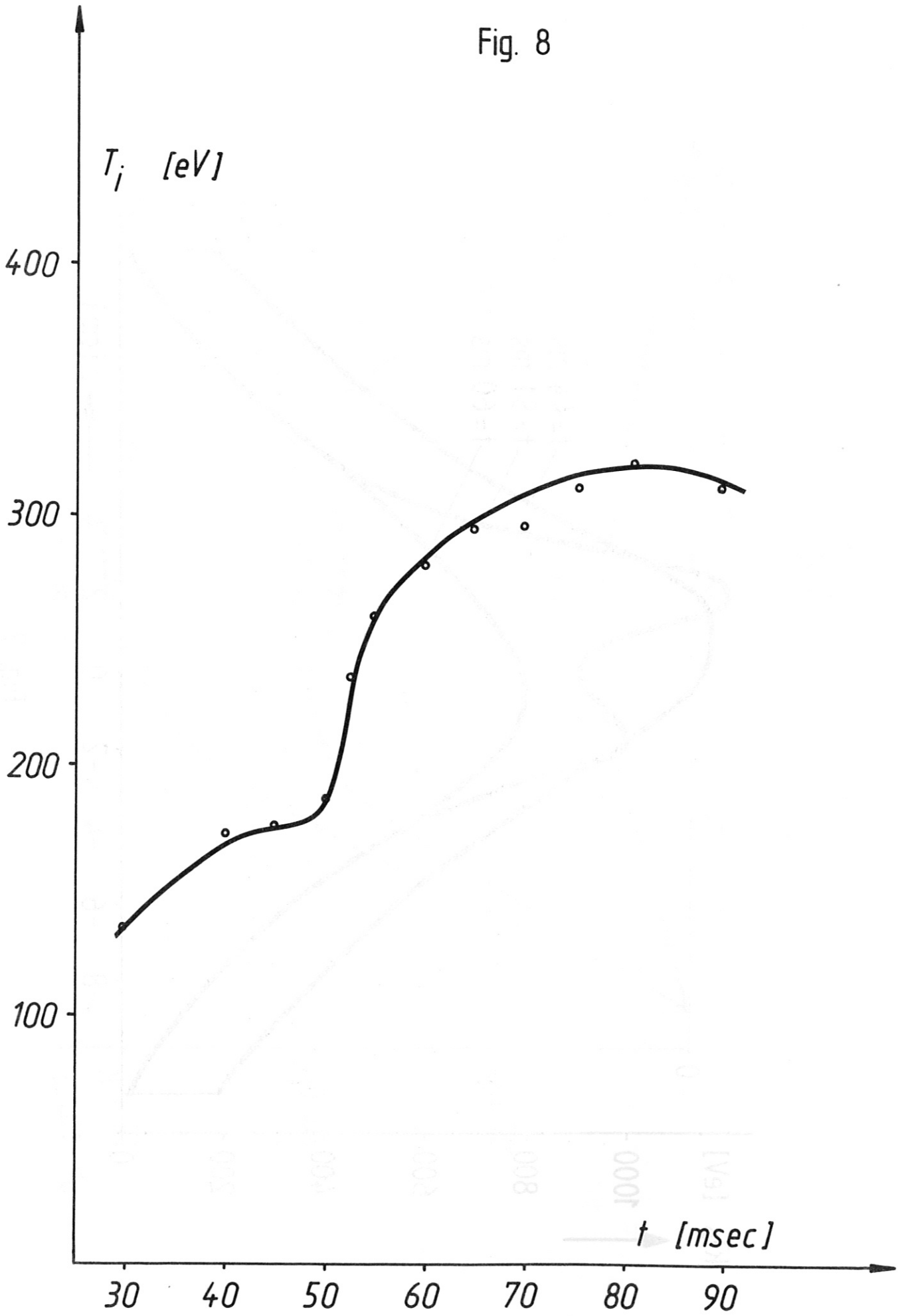

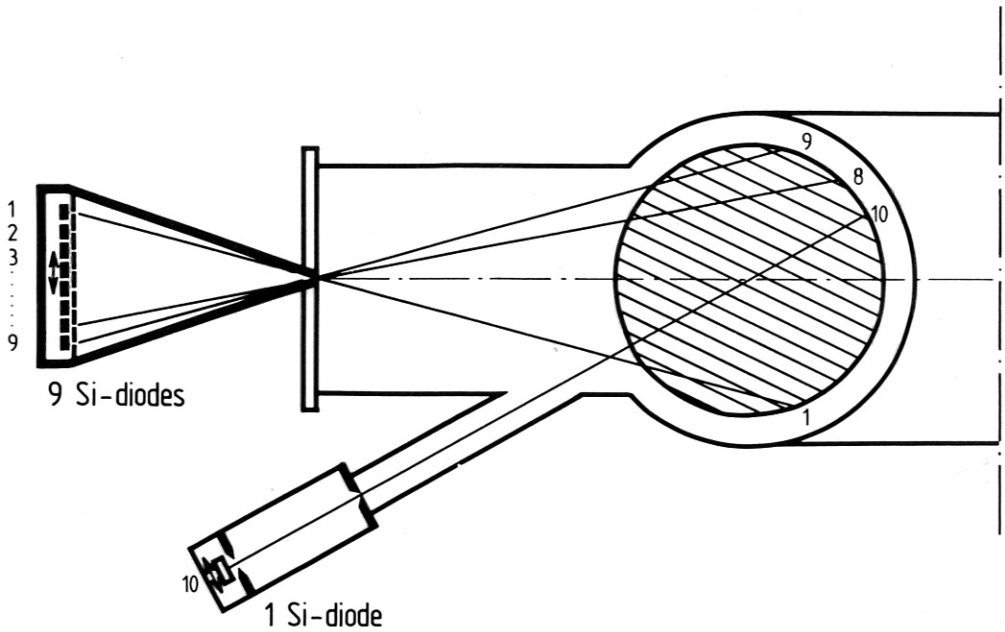
1
2
3
9
9 Si-diodes
9
8
10
1
10
1 Si-diode

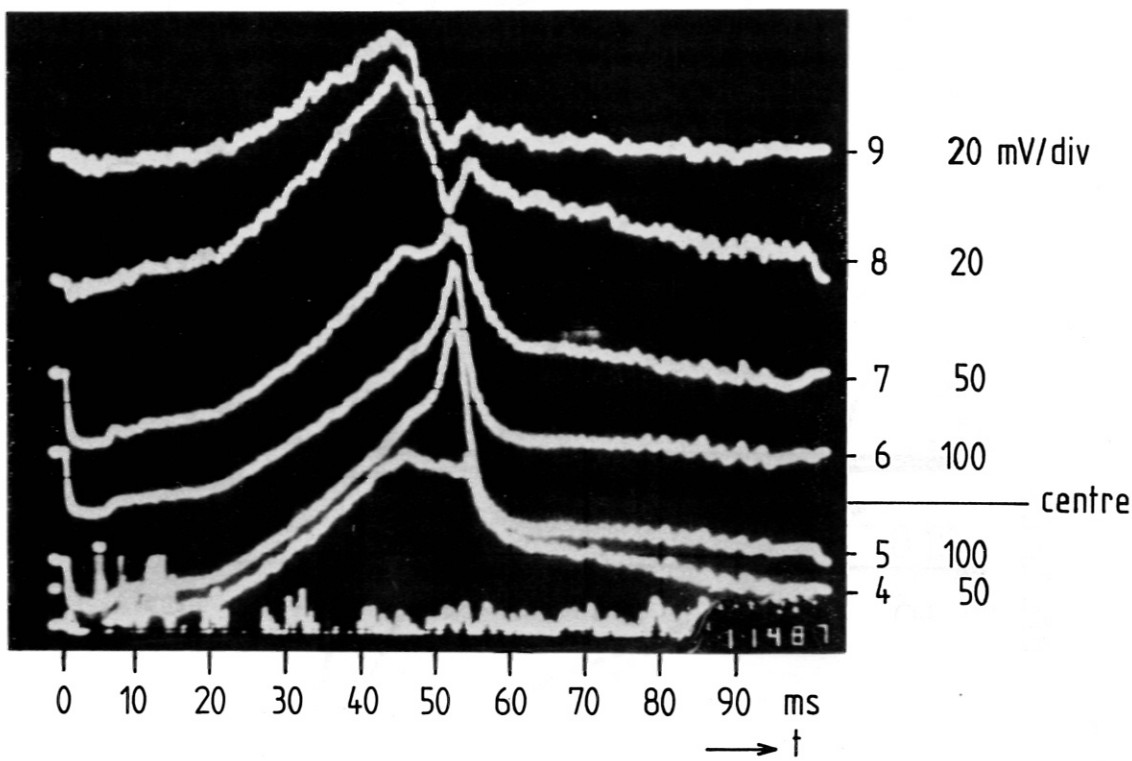
9 20 mV/div
8 20
7 50
6 100
centre
5 100
4 50
0 10 20 30 40 50 60 70 80 90 ms
t

Fig. 9

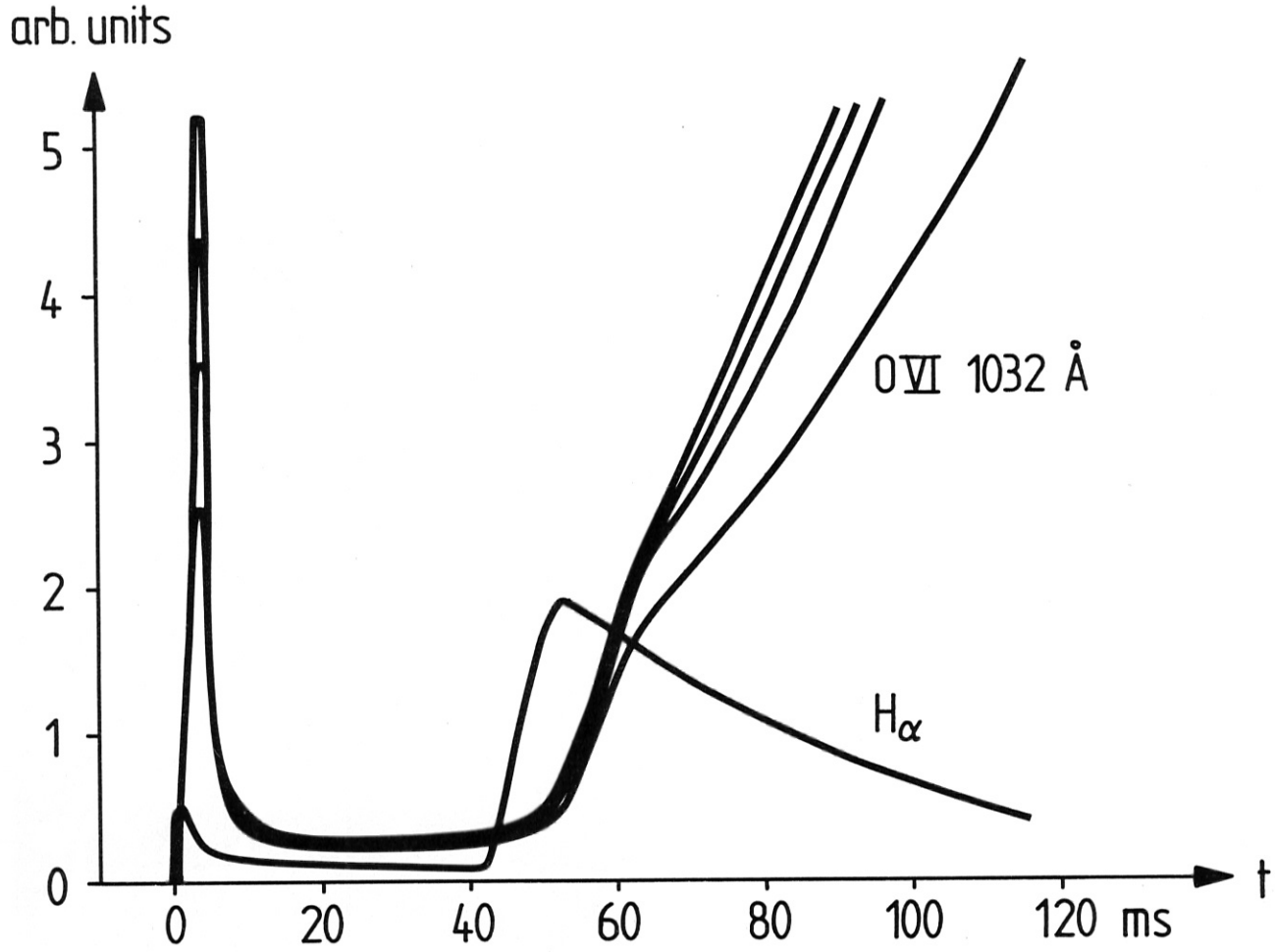

Fig. 10

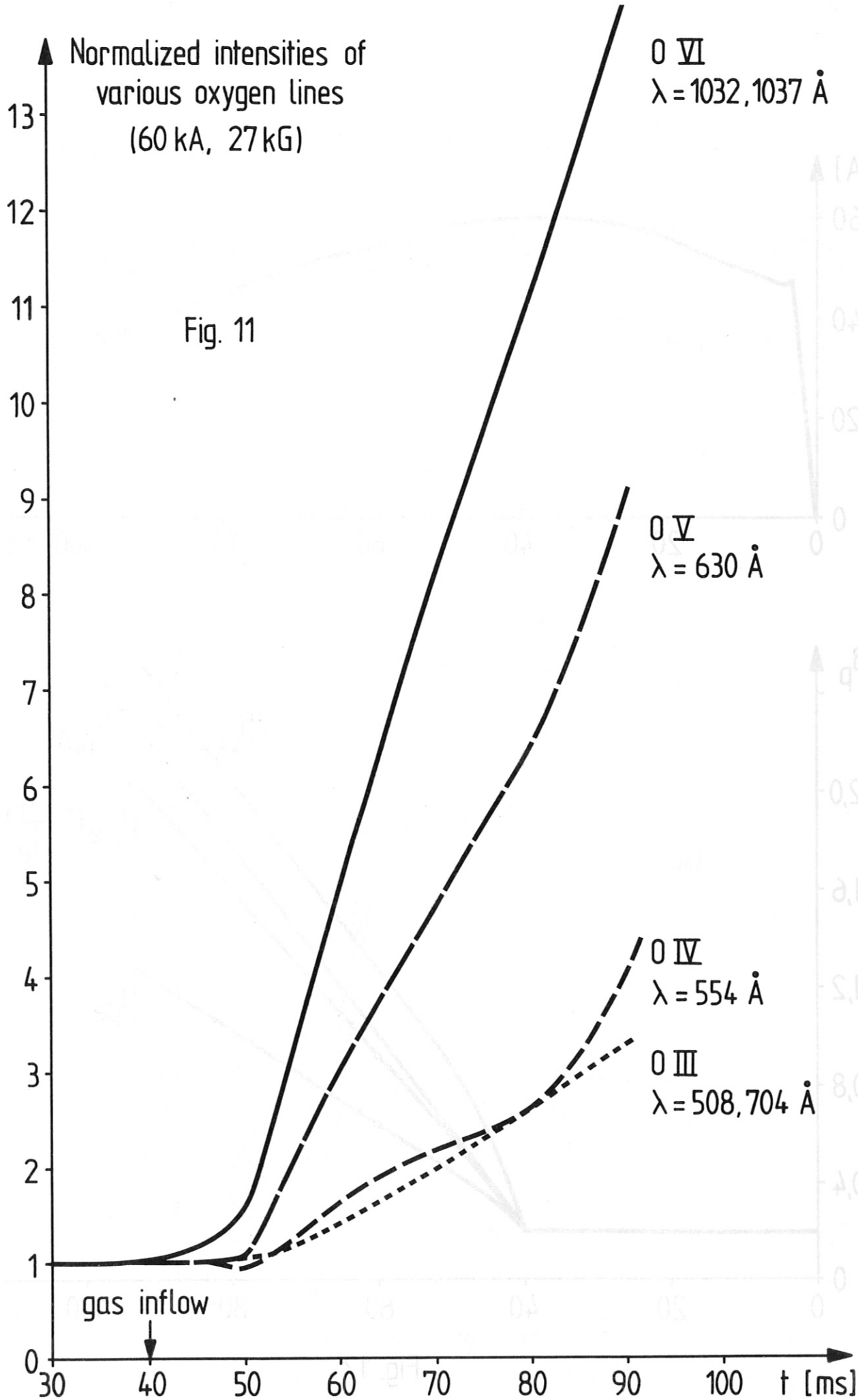
Normalized intensities of
various oxygen lines
(60 kA, 27 kG)
O VI
λ = 1032, 1037 Å
O V
λ = 630 Å
O IV
λ = 554 Å
O III
λ = 508, 704 Å
gas inflow
0
1
2
3
4
5
6
7
8
9
10
11
12
13
30
40
50
60
70
80
90
100
t [ms]

Fig. 11

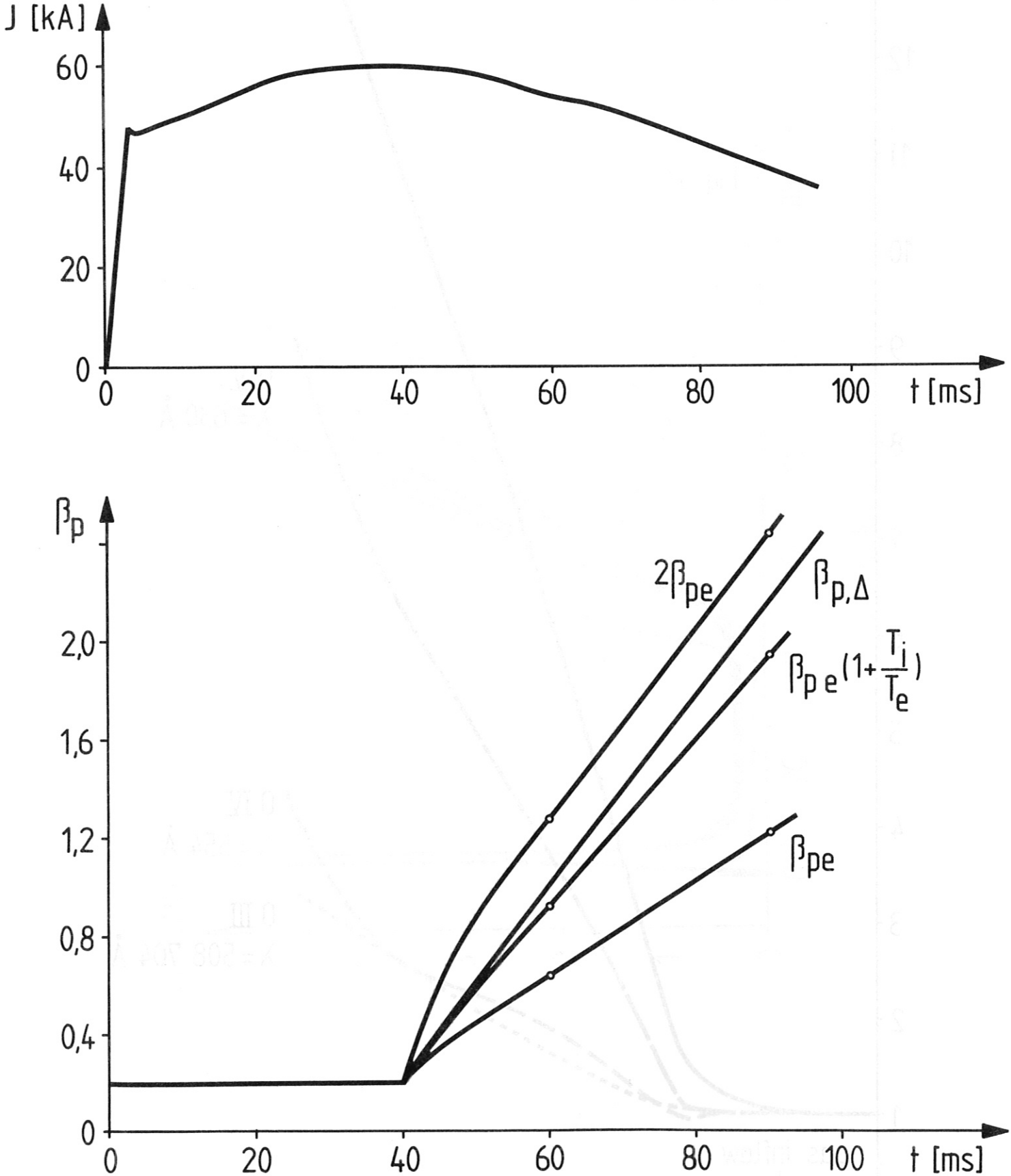
J [kA]
60
40
20
0
0
20
40
60
80
100
t [ms]

β_p
2,0
1,6
1,2
0,8
0,4
0
$2\beta_{pe}$
$\beta_{p,\Delta}$
$\beta_{p\,e}(1+\frac{T_i}{T_e})$
β_{pe}
0
20
40
60
80
100
t [ms]

Fig. 12

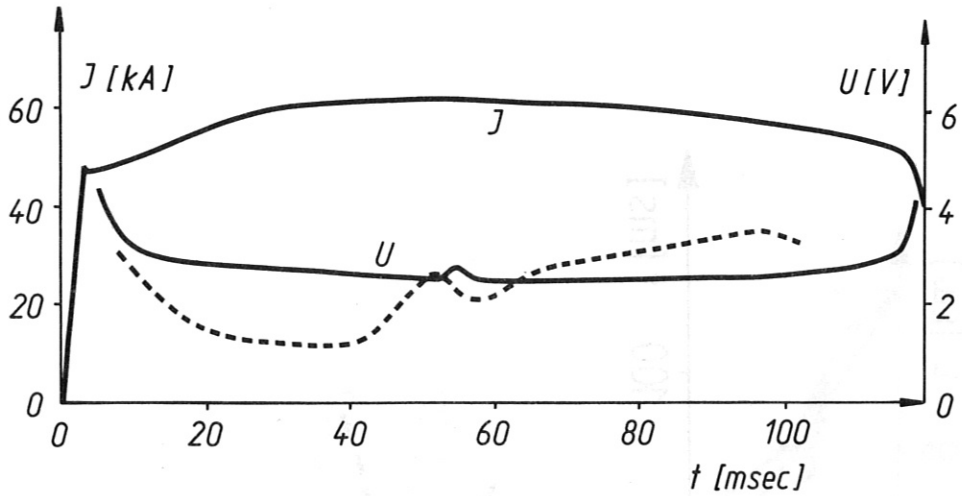
J [kA]
U [V]
J
U
60
40
20
0
6
4
2
0
0
20
40
60
80
100
t [msec]

Fig. 13

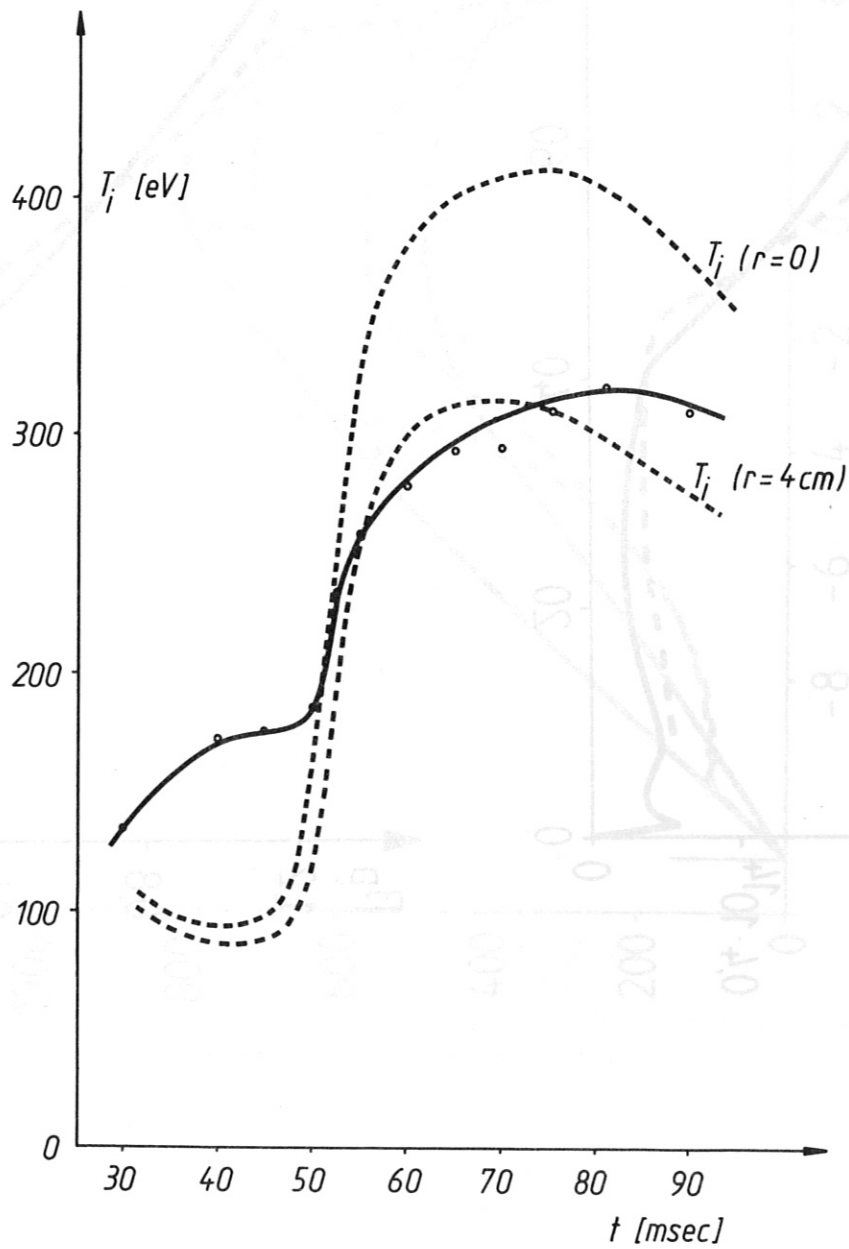
T_i [eV]
400
300
200
100
0
T_i (r=0)
T_i (r=4cm)
30
40
50
60
70
80
90
t [msec]

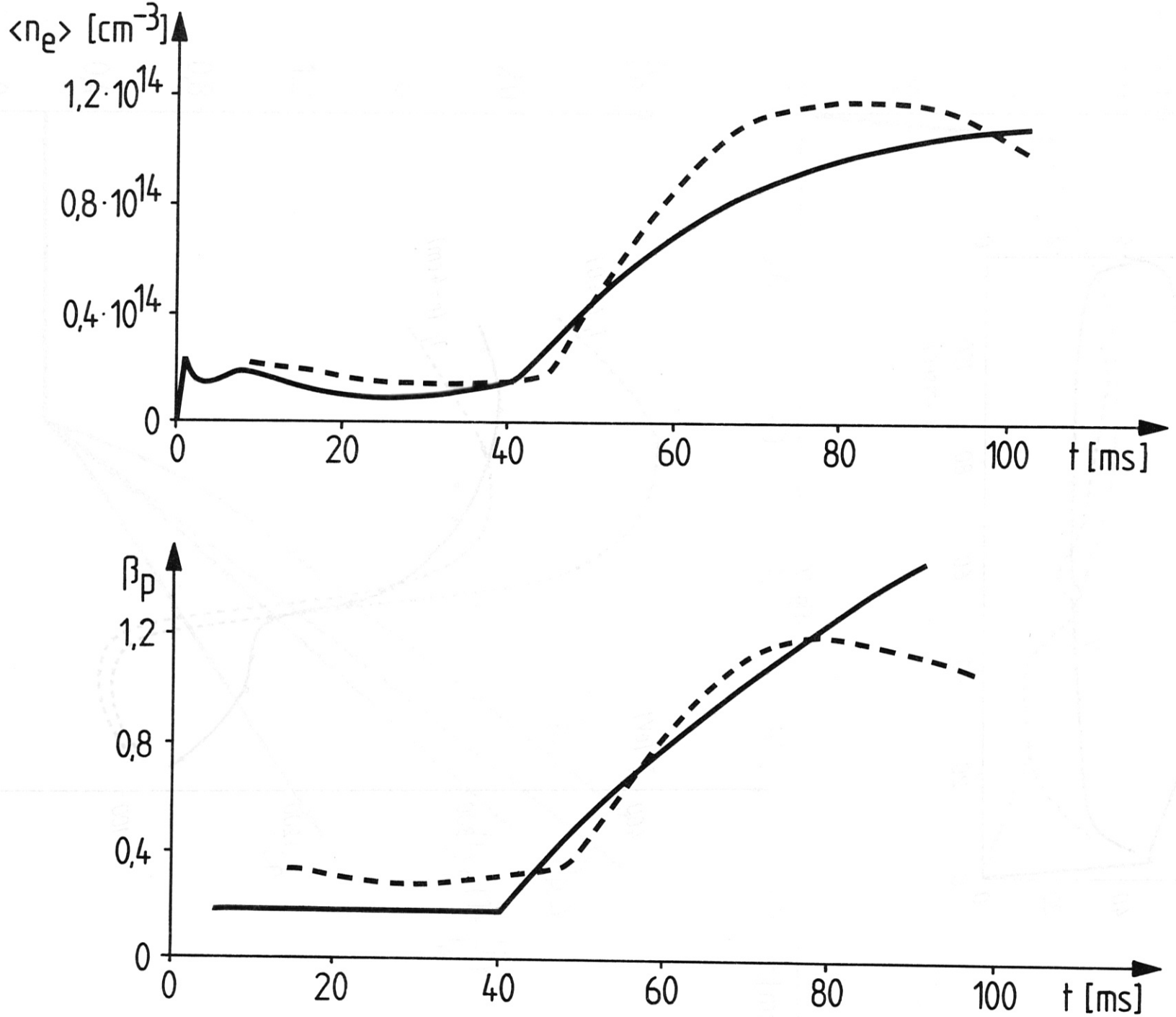
$\langle n_e \rangle$ [cm^{-3}]
1,2·10^{14}
0,8·10^{14}
0,4·10^{14}
0
0
20
40
60
80
100
t [ms]
β_p
1,2
0,8
0,4
0
0
20
40
60
80
100
t [ms]

Fig. 14

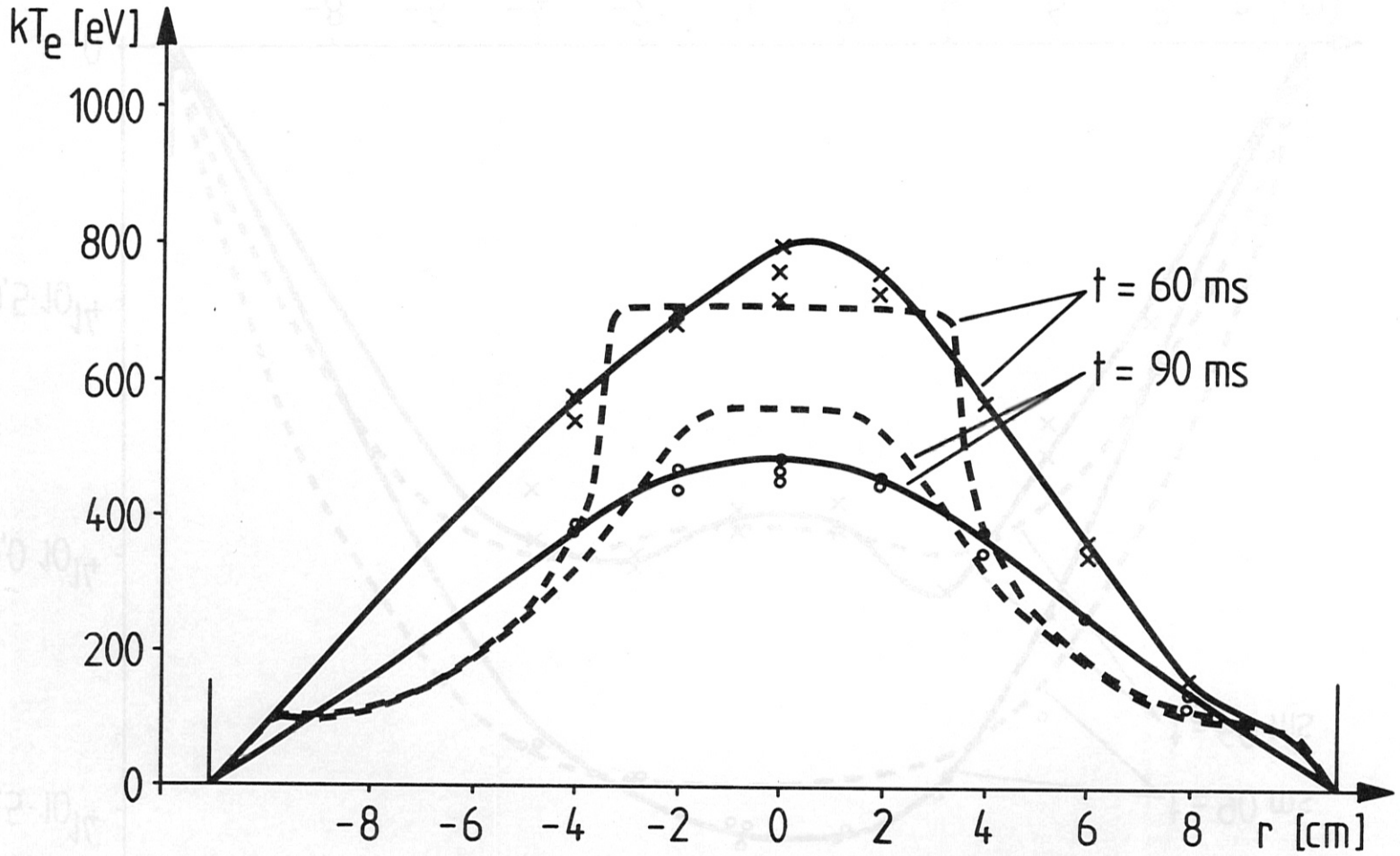

Fig. 15

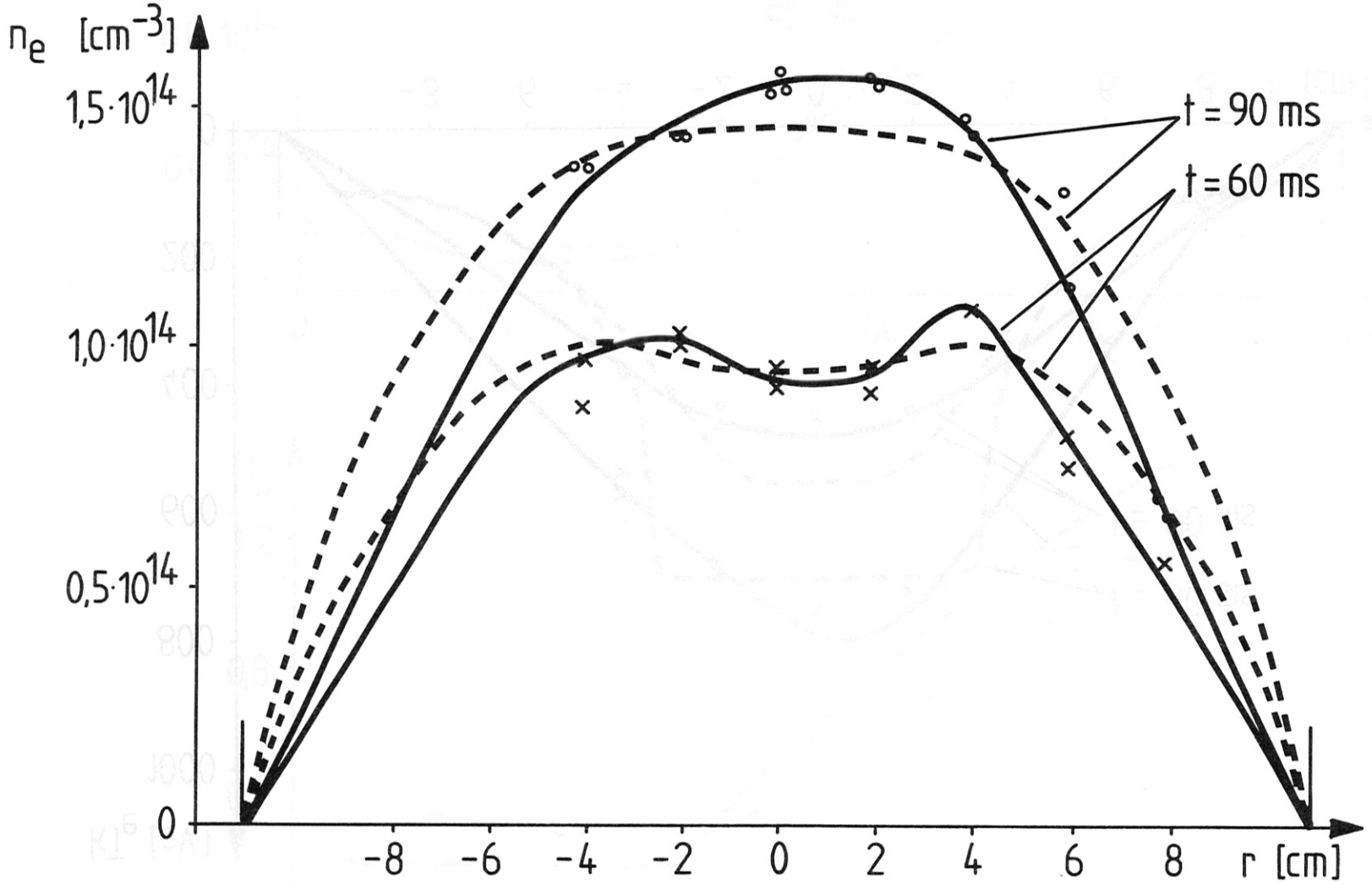
n_e [cm^{-3}]
$1{,}5 \cdot 10^{14}$
$1{,}0 \cdot 10^{14}$
$0{,}5 \cdot 10^{14}$
0
t = 90 ms
t = 60 ms
-8
-6
-4
-2
0
2
4
6
8
r [cm]

Fig. 16